Bulletin of the JSME Vol.11, No.2, 2017
Journal of Advanced Mechanical Design, Systems, and Manufacturing

Optimization of 3-DOF parallel motion devices for low-cost vehicle simulators

Sergio CASAS*, Inmaculada COMA*, Cristina PORTALÉS* and Marcos FERNÁNDEZ*
*IRTIC, Universitat de València, C/ Catedrático José Beltrán 2, 46980, Paterna (Valencia), Spain
E-mail: Sergio.Casas@uv.es

Received: 5 October 2016; Revised: 17 April 2017; Accepted: 15 May 2017

Abstract
Motion generation systems are becoming increasingly important in certain Virtual Reality (VR) applications, such as vehicle simulators. This paper deals with the analysis of the Inverse Kinematics (IK) and the reachable workspace of a three-degrees-of-freedom (3-DOF) parallel manipulator, proposing different transformations and optimizations in order to simplify its use with Motion Cueing Algorithms (MCA) for self-motion generation in VR simulators. The proposed analysis and improvements are performed on a 3-DOF heave-pitch-roll manipulator with rotational motors, commonly used for low-cost motion-based commercial simulators. The analysis has been empirically validated against a real 3-DOF parallel manipulator in our labs using an optical tracking system. The described approach can be applied to any kind of 3-DOF parallel manipulator, or even to 6-DOF parallel manipulators. Moreover, the analysis includes objective measures (*safe zones*) on the workspace volume that can provide a simple but efficient way of comparing the kinematic capabilities of different kinds of motion platforms for this particular application.

Key words: Kinematic analysis, Parallel manipulator, Motion platform, Motion simulation, 3-DOF

1. Introduction

Human-computer interactions can be really complex in simulation systems where a believable motion generation is needed for the fulfilment of the simulation goals. The use of motion platforms to add inertial cues can significantly enhance the user immersion in the simulator, provided the system is properly tuned (Casas et al., 2016; Nahon and Reid, 1990; Reid and Nahon, 1986). The understanding of motion platforms' behavior and functioning is necessary to design effective and immersive experiences with this kind of simulators. In this regard, there are several works in the literature focused on the analysis of the behavior of several motion mechanisms with different features. However, it is hard to find research works focused on the peculiarities of the usage of motion platforms for motion generation in real-time vehicle simulation, which is the main target of this contribution.

One of the most important features of motion platforms when used in vehicle simulators is the amount of linear and angular displacement the device is able to provide over the different axes. These features are crucial since they can affect the physical validity of the simulator (Reymond and Kemeny, 2000) and enhance/reduce the magnitude distortion (Sinacori, 1977) of the generated perceptual cues. In consequence, they condition the experience of the simulators' users (Casas et al., 2015). These features are generally known in the literature as the *workspace*. This workspace can be expressed in terms of a Cartesian space or in terms of the amount of degrees-of-freedom (DOF) the manipulator is able to reach. For motion simulation, it is much more interesting to analyze it in terms of DOF-space due to the fact that motion platforms are usually designed based on the DOF, rather than in absolute positions.

The goal of these motion platforms is to provide the user with the most suitable perception of driving/piloting the real vehicle that is being simulated. These systems try to reproduce the response of the vehicle to driver inputs by using a set of translational and angular movements that represent the motion cues a driver would perceive in real conditions. However, a motion platform is invariably constrained by its mechanical limits. Therefore, the response must be filtered to avoid reaching the physical limits of the mechanism, causing the generation of false cues. In consequence, one of the decisive factors for designing an immersive experience is the analysis of the ranges and the interdependence between the

Paper No.16-00547
[DOI: 10.1299/jamdsm.2017jamdsm0023]

excursions along the different DOF available in the motion platform.

Manipulators can be classified in serial and parallel (L.-W. Tsai, 1999). Over the last years, the advantages of parallel manipulators (PM) in terms of high accuracy, velocity, stiffness and payload capacity over the serials, have promoted their use not only for motion simulation but also for a wide variety of applications (Merlet, 2006). However, PM also expose disadvantages like their relatively limited workspace and the difficulty of the calculation of the forward kinematics formulation.

The most common mechanisms for motion simulation are the 6-DOF PM. Most of them are based on the Gough-Stewart platform architecture (Stewart, 1965). Several researchers have addressed the analysis of the Gough-Stewart platform, developing kinematic and dynamic analyses (Cheng et al., 2003; Dasgupta and Mruthyunjaya, 2000), presenting algorithms for solving the forward kinematics problem (Korobeynikov and Turlapov, 2005; Liu et al., 1993), studying the workspace (Li et al., 2007; Majid et al., 2000) or optimizing the platform design. Although the 6-DOF Stewart hexapod is a de facto standard, this device is not always required to achieve a good immersive experience and in many cases it may be unaffordable. In fact, recent approaches (Arioui et al., 2009; Dingxuan et al., 2001; Nehaoua et al., 2008) focus on radically different strategies based on the use of limited-DOF mechanisms that both maintain the inherent advantages of PM while providing other advantages in terms of cost reduction in manufacturing and simpler mechanical design. This reduction in cost has motivated this research work.

The cost of a motion platform is mainly driven by the cost of its actuators. Usually, *n*-DOF devices require *n* actuators. If limited-DOF devices are used, the cost of the simulator could significantly decrease. Assuming similar sizes and powers, a 6-DOF PM could be almost twice as expensive as a 3-DOF mechanism. The challenge is to choose the device so that the cost is significantly reduced but the performance of the simulator does not. If properly built, the differences between a 3-DOF device and a 6-DOF mechanism could be fairly small (Pouliot et al., 1998). In this regard, a heave-pitch-roll mechanism, despite having only three DOF, is able to generate perceptual motion cues up to five of the six possible DOF: three by physical motion, plus two simulated DOF taking advantage of the somatogravic illusion (MacNeilage et al., 2007) by means of the tilt-coordination technique (Groen and Bles, 2004).

Many 3-DOF translational PM and their kinematic analysis have been proposed with various topologies, like 3-UPU (L. Tsai and Joshi, 2000), 3-URC (Di Gegorio, 2001), 3-RRC (Zhang et al., 2009), 3-CRR (Kong and Gosselin, 2002), 3-RPC (Callegari and Tarantini, 2003), a Cartesian parallel manipulator (Kim, 2006), 3-RCC (Callegari et al., 2006) and many others. Although translational mechanisms have received more attention than others, there are several designs with other topologies including rotational PM. For instance, Zhang et al. (2009) developed an uncoupled T2R1 manipulator applied in parallel vibration sieve, Richard et al. (2007) designed a 4-DOF T3R1 partially decoupled and Gogu (2006) proposed an approach for structural synthesis of fully-isotropic T3R2 parallel manipulators.

Despite the great number of works on the subject, to the best of our knowledge there is not any published analysis regarding the low-cost commercial manipulator we describe in this contribution, consisting of one translational DOF and two rotational DOF. Moreover, we have also found a clear lack of research works focused on motion simulation. This has been the main motivation of our research and the main distinguishing aspect with respect to other works. The main contribution of this paper is the analysis of the relationships between the different DOF of a 3-DOF PM used for motion simulation. The analyzed device is a common heave-pitch-roll (T1R2 – 1 translational, 2 rotational DOF) PM design for low-cost motion cueing. This contribution may be welcome in applications where 6-DOF solutions are not affordable or where movable simulators are needed to ease the transportability and the construction of the simulator.

The rest of the paper is organized as follows. Section 2 describes the manipulator while section 3 briefly studies the solution to the Inverse Kinematics problem. Section 4 deals with the validation of the equations. In Section 5, the workspace is first analyzed and then improved in order to simplify the use of this PM for motion simulation. Finally, some conclusions are drawn and exposed in Section 6.

2. Manipulator design and description

The motion platform analyzed in this paper is a 3-DOF T1R2 parallel manipulator with the following degrees of freedom: heave (Z-axis translation), pitch (X-axis rotation) and roll (Y-axis rotation). It is composed of three rotational motors, three connecting rods, three pistons, a vertical splined shaft and a *moving base* (see Fig. 1a, where elements in white are movable parts, and the rest are static). The names *connecting rod* and *piston* are used instead of more anthropomorphic terms like arm, leg or limb, as an analogy to a combustion engine, for their functioning is similar to a

[DOI: 10.1299/jamdsm.2017jamdsm0023]

rod-piston (slider-crank) system (although they are not exactly equivalent, since in this T1R2 mechanism the piston does not always move in a straight line). This architecture is typical in some low-cost commercial simulators (InMotion, 2017; Simulation, 2017). The use of rotational motors makes the mechanism more affordable and suitable for low-cost vehicle simulators, since electrical rotational motors are more common than linear motors.

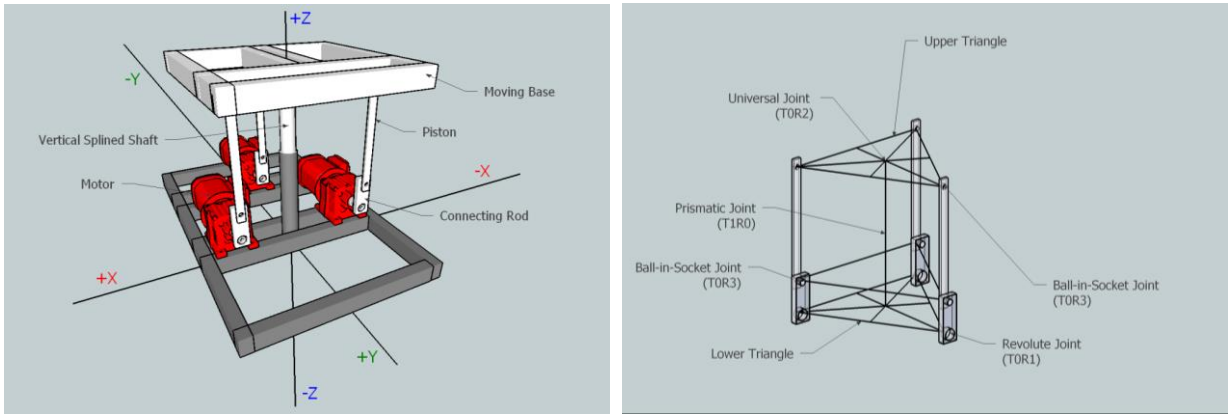

Fig. 1. a) The 3-DOF T1R2 parallel manipulator analyzed in this paper. b) Joints and movable elements of this device.

The kinematic chains of this parallel manipulator are arranged in a parallel manner as depicted in Fig. 1. Each motor axis is linked to a connecting rod by means of a T0R1 revolute joint, so that all three connecting rods are actuated (they transmit the angular motion of the motors). Each motor can be individually controlled, so that connecting rods can form a different angle with the horizontal XY plane. The three connection points of the motors with the connecting rods are arranged in a triangular shape. As the motors rotate around their axes, but do not change their Cartesian position, this triangle has always the same shape and size. The vertices of this triangle are denoted by $\overrightarrow{L_1}$, $\overrightarrow{L_2}$, $\overrightarrow{L_3}$ and the triangle is referred to as the *lower triangle* (see Fig. 1b and Fig. 2a). As the connecting rods can only move on a vertical XZ plane (because of the revolute joint), the ends of the three connecting rods form another triangle. The vertices of this triangle are denoted by $\overrightarrow{X_1}$, $\overrightarrow{X_2}$, $\overrightarrow{X_3}$. This triangle is not static, because it can change its position and even its shape, as the connecting rods move. Each rod is linked to a piston (of length p) by means of a T0R3 spherical joint at $\overrightarrow{X_1}$, $\overrightarrow{X_2}$, $\overrightarrow{X_3}$. Similarly, each piston is linked to the moving base by another T0R3 spherical joint at $\overrightarrow{U_1}$, $\overrightarrow{U_2}$, $\overrightarrow{U_3}$. These three points constitute another triangle, which is referred to as the *upper triangle* (see Fig. 2). Since the moving base is rigid, this triangle can move and rotate, but it cannot change its shape. The position and orientation of this upper triangle is important, as it will define the heave, pitch and roll of the parallel manipulator. The sphere in Fig. 2a represents the possible positions of the piston (when it rotates around $\overrightarrow{U_3}$), and the vertical XZ circle represents the possible positions of $\overrightarrow{X_3}$ (when it rotates around $\overrightarrow{L_3}$). Although it is not drawn for simplicity, the same can be applied to $\overrightarrow{U_1}$, $\overrightarrow{U_2}$, $\overrightarrow{L_1}$, $\overrightarrow{L_2}$, $\overrightarrow{X_1}$, $\overrightarrow{X_2}$.

As both piston joints are spherical joints with full rotational freedom, more joints are needed to prevent the motion platform from rotating uncontrolledly around the Z-axis (yaw rotation) and from moving along the X and Y axes (surge and sway). This is accomplished by a T0R2 universal joint placed at the barycenter of the upper triangle, and by a vertical splined shaft linked to the universal joint. The choice of the barycenter is not arbitrary. This point is the center of mass of the triangle, so it is the place where the weight of the motion base is equally distributed. The universal joint allows the moving base to perform pitch and roll rotations. The vertical splined shaft acts as a T1R0 prismatic joint, allowing the moving base to move along the Z-axis, while avoiding any yaw, surge or sway motions. These two joints are usually built separately, but they can be conceptually treated as a T1R2 prismatic universal joint. The vertical axis can also be equipped with a spring. The spring can be helpful to ease the lifting process of the moving base, when the motors are not powerful enough, but it does not change the kinematic properties of the mechanism.

[DOI: 10.1299/jamdsm.2017jamdsm0023]

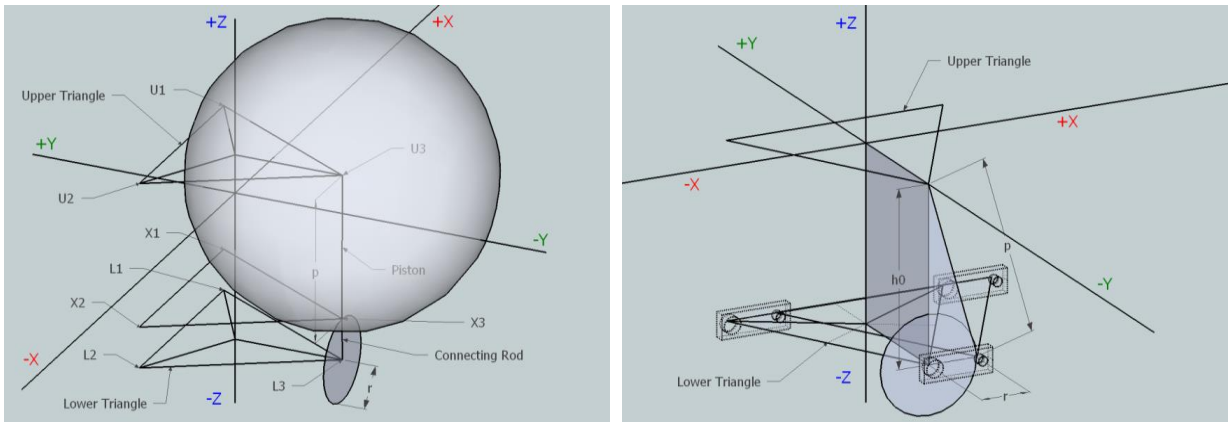

Fig. 2. a) Geometrical model showing the triangles, a rod and a piston. The sphere and the circle represent possible positions of the piston and rod respectively b) Coordinate system and home position. The center of the coordinate system is located at the barycenter of the upper triangle. The motors are in horizontal position (0º) looking right.

In parallel mechanism terminology, this device is a 3-RSSUP parallel manipulator, as there are three kinematic chains, each composed of an actuated revolute joint, two spherical joints, a universal joint and a prismatic joint. As our main interest is the applied use of this technology and not the analysis of the kinematic chains, the parallel manipulator is referred to as 3-DOF or T1R2, because it reflects best its application and the possible uses of this motion device.

Of course, to perform any kind of kinematic study, we need to define a coordinate system. In this case, the most natural point to place the origin of the coordinate system is the center of the upper triangle, when the motion platform is at the so-called *home position*. The home position is usually chosen to be the motion platform pose (position + orientation) that results when all the motor axes are in horizontal position. The coordinate system is depicted in Fig. 2b.

3. Inverse Kinematics

Inverse Kinematics (IK) is the process and equation system that needs to be solved to calculate the target angles for the motors (the position of the actuators in a general case) in order to achieve a desired set of DOF. IK needs to be solved when the target angles for the motors are unknown but the desired pose (position + orientation) of the motion platform, expressed as a set of DOF, is known. The natural use of a motion platform for motion cueing generation takes the following steps. First, a physics model of the simulated entity calculates the dynamic state of the simulated system. Next, a Motion Cueing Algorithm (MCA) decides a new set of DOF for the motion platform, using the state (speed, force, etc.) of the simulated entity as an input. Afterwards, the target angles for the motors are calculated by the IK. These desired angles feed the motors controllers and change the set-point of the controllers. Finally, the controllers calculate the amount of torque necessary to move the motors towards their desired destinations. When the motors reach these angles, the motion platform pose should match the desired set of DOF calculated by the MCA. However, it is often the case that the desired set of DOF is physically unreachable. Thus, it is desirable that the IK detect this case.

Considering this, the input/output specification of the IK of a rotational 3-DOF mechanism is the following. The IK inputs are: *target* (desired) *heave*; *target pitch*; *target roll*. The IK outputs are: *feasible* (yes/no), to detect unreachable poses; α_k: angle of motor k (where $k = 0, 1, 2$ represents each of the involved motors) with respect to the horizontal plane. As the connecting rod is attached to the motor, this angle is the angle between the connecting rod and the XY plane. Rod angles are measured in the usual way: counter-clockwise with 0° at the 3 o'clock position (facing $+X$).

From Fig. 2a, we can also identify the different parameters of the system: r is the length of the connecting rods; p is the piston length; $\overrightarrow{L_k}$ is the position of the lower triangle vertices (the position of the motors) and $\overrightarrow{U_{k0}}$ is the initial position of the upper triangle vertices, $\overrightarrow{U_k}$. In the case of the T1R2 motion platform being analyzed, these parameters suffer some restrictions due to the particular design of this parallel manipulator: (i) $p > r$ (otherwise, the upper triangle will eventually collide with the lower triangle); (ii) upper and lower triangles are isometric (of equal shape and size); (iii) upper and lower triangles are at least isosceles; (iv) upper and lower triangles are aligned on the Z-axis when $\alpha_k = 90°$.

The home position of the motion platform can be arbitrarily chosen. One possible choice is to define the home position when the motors are in horizontal position ($\alpha_k = 0$). This position will be considered to be the $(0, 0, 0)$ pose (i.e. heave = 0 m, pitch = 0°, roll = 0°). At this home position, the distance between the upper and the lower triangle (h_0)

[DOI: 10.1299/jamdsm.2017jamdsm0023]

can be calculated using the Pythagoras rule (see Fig. 2b):

$$h_0 = \sqrt{p^2 - r^2} \tag{1}$$

As aforementioned, the goal of IK is to obtain α_k $(k = 0, 1, 2)$ from heave, pitch and roll, respectively. To that end, we need first to calculate the position of $\overrightarrow{U_k}$ for a given heave, pitch and roll. It is clear that $\overrightarrow{U_k} = \overrightarrow{U_{k0}}$ at home position. However, when the moving base (upper triangle) moves, $\overrightarrow{U_k}$ needs to be recalculated:

$$\overrightarrow{U_k} = R_x R_y \overrightarrow{U_{k0}} + \overrightarrow{(0,0,heave)} \tag{2}$$

where the rotation matrices R_x and R_y are defined as:

$$R_x = \begin{bmatrix} 1 & 0 & 0 \\ 0 & cp & sp \\ 0 & -sp & cp \end{bmatrix}, \text{ where } \quad cp = \cos(pitch), \quad sp = \sin(pitch) \tag{3}$$

$$R_y = \begin{bmatrix} cr & 0 & -sr \\ 0 & 1 & 0 \\ sr & 0 & cr \end{bmatrix}, \text{ where } \quad cr = \cos(roll), \quad sr = \sin(roll) \tag{4}$$

The position of the vertices of the lower triangle $(\overrightarrow{L_k})$ can be calculated with respect to the upper triangle points $(\overrightarrow{U_k})$:

$$\overrightarrow{L_k} = \overrightarrow{U_{k0}} - \overrightarrow{(0,0,h_0)} - \overrightarrow{U_k} \tag{5}$$

It is important to emphasize that, although $\overrightarrow{L_k}$ do not move, these variables are calculated with respect to $\overrightarrow{U_k}$, and, thus, $\overrightarrow{L_k}$ will change if the manipulator moves. This decision simplifies further equations. Given $\overrightarrow{L_k}$, if its Z-component is positive, then a physically-absurd solution exists (but mathematically plausible) with the upper triangle below the lower one. This solution is marked as *not feasible* and solved as $\alpha_1 = \alpha_2 = \alpha_3 = -90°$, because it is the closest possible solution. If the Z-component of $\overrightarrow{L_k}$ is negative, the place where the piston and the connecting rod match (if they do) needs to be calculated. To do this, the intersection of a sphere, of radius p, around $\overrightarrow{U_k}$ with a vertical XZ circle, of radius r, around $\overrightarrow{L_k}$ is calculated (see Fig. 2a). This is where the decision to express $\overrightarrow{L_k}$ relative to $\overrightarrow{U_k}$ really pays off, as we can define the sphere centered at $(0, 0, 0)$ and the circle centered at $\overrightarrow{L_k}$, which is much simpler than writing the sphere centered at a non-zero point. This trick is a simple but effective contribution to the solution of the IK, and constitutes a differentiating point of our work. As the equation is quadratic, there can be up to two valid solutions: $\overrightarrow{X_{k1}}$ and $\overrightarrow{X_{k2}}$. These two solutions arise from solving the intersection of the sphere and the circle:

$$(\overrightarrow{X_{k1}},\ \overrightarrow{X_{k2}},\ \text{feasible}) = \text{DualSphereCircleIntersection}\left(p, r, \overrightarrow{L_k}\right) \tag{6}$$

As both $\overrightarrow{X_{kJ}}$ and $\overrightarrow{L_k}$ are expressed in the same coordinate system (both with respect to $\overrightarrow{U_k}$), the subtraction of these points immediately provides the two possible orientation vectors of the connecting rod (let us call them $\overrightarrow{B_{k1}}$ and $\overrightarrow{B_{k2}}$):

$$\begin{cases} \overrightarrow{B_{k1}} = \overrightarrow{X_{k1}} - \overrightarrow{L_k} \\ \overrightarrow{B_{k2}} = \overrightarrow{X_{k2}} - \overrightarrow{L_k} \end{cases} \tag{7}$$

Finally, these two vectors give the two final possible angles for the motors, which is the final goal of IK:

$$\begin{cases} \alpha_{k1} = \tan^{-1}(B_{k1z}/B_{k1x}) \\ \alpha_{k2} = \tan^{-1}(B_{k2z}/B_{k2x}) \end{cases} \tag{8}$$

As shown, the solutions are always dual because the sphere-circle intersection always gives, if they exist, two different solutions (except for the singularities, which will be addressed later, where both solutions are equal). The process of calculating the sphere-circle intersection requires some further mathematical explanation. Let us call $\overrightarrow{(x, y, z)}$ the point(s) where a sphere of radius p around $\overrightarrow{(0, 0, 0)}$ and a vertical XZ circle of radius r around $\vec{L}$, intersect:

$$\overrightarrow{(x, y, z)} = \text{SphereCircleIntersection}(p, r, \vec{L}) \tag{9}$$

The equation system is:

[DOI: 10.1299/jamdsm.2017jamdsm0023]

$$\begin{cases} x^2 + y^2 + z^2 = p^2 \\ (x - L_x)^2 + (z - L_z)^2 = r^2 \\ y = L_y \end{cases} \tag{10}$$

The solutions of this equation system are:

$$\begin{cases} y = L_y \\ x = \dfrac{-r^2 {L_x}^2 + {L_x}^2\left({L_x}^2 + {L_z}^2 + p^2 - y^2\right) \pm L_z a}{2L_x({L_x}^2 + {L_z}^2)} \\ z = \dfrac{-r^2 L_z + L_z\left({L_x}^2 + {L_z}^2 + p^2 - y^2\right) \pm a}{2({L_x}^2 + {L_z}^2)} \end{cases} \tag{11}$$

where

$$a = \sqrt{-{L_x}^2\left(r^4 - 2r^2\left({L_x}^2 + {L_z}^2 + p^2 - y^2\right) + \left({L_x}^2 + {L_z}^2 - p^2 + y^2\right)^2\right)} \tag{12}$$

If a is a complex number, there is no physical solution, as the piston cannot reach the rod at the desired DOF. In this case, *feasible* will be marked as false. Otherwise, the sphere-circle intersection is solved (therefore *feasible* will be true), which immediately leads to the dual solutions of the IK. The singularities caused when L_x approaches 0 must be taken into to account, because this produces an indetermination in x, which is settled by solving the following limit:

$$\lim_{L_x \to 0} x = \pm \frac{\sqrt{-r^4 + 2r^2\left({L_z}^2 + p^2 - y^2\right) - \left({L_z}^2 - p^2 + y^2\right)^2}}{2L_z} \tag{13}$$

Again, if x is a complex number (the radicand is negative), there are no possible physical solutions.

4. Validation of the Inverse Kinematics

To perform the validation of the IK formulation provided in the previous section, a particular instance of the T1R2 motion device was built. The following parameters were selected, which represent a typical set-up of a low-cost small-sized motion simulation system: p = 0.35 m; r = 0.1 m; equilateral triangle of side 0.45 m, centered on its barycenter. A real motion platform (an instance of this 3-DOF design) following this parameter set-up was built in our lab in order to empirically validate the results presented in this work. A picture of the constructed device can be seen in Fig. 3.

To perform the validation of the IK formulation presented in this work, we used an optical tracking system, composed of six *Natural Point Optitrack V100:R2* cameras. This is a passive optical tracking system that uses markers coated with a retro-reflective material that reflects the infrared light generated near the cameras' lens (Fig. 3 shows an example of a marker placed on the moving base). The capture settings of the cameras can be adjusted so that only the bright reflective markers are captured, ignoring any other materials. This optical system allows us to validate the real response of the PM against the proposed IK formulation with an error lower than 2 millimeters, which is the measuring error imposed by the cameras' system, given a proper calibration and set-up. The validation has been carried out by implementing the IK in C++ and analyzing the three DOF separately (heave, pitch and roll), comparing the actual response of the system with the expected response represented by the IK equations. Figure 4 shows the results obtained with our motion platform. The blue dashed lines correspond to the theoretical model provided by the equations, whereas the green lines correspond to the real response of the system. As the reader can see, the desired DOF are obtained with almost a 100% accuracy. Needless to say, the motion platform takes some time to reach its desired pose. This time is roughly half a second in our tests, but for the validation of the IK formulation, it is not relevant. It includes a small transport delay, the latency of the optical tracking system and the inertia of the motion system. Once this transient is over, the stationary behavior shows very small differences between the expected pose and the real one. The differences arise because of construction errors (impossible to measure), motor positioning errors (should be fairly small as we used *SEW-Eurodrive* motors equipped with high resolution absolute encoders) and the optical measurement accuracy (less than 2 millimeters).

[DOI: 10.1299/jamdsm.2017jamdsm0023]

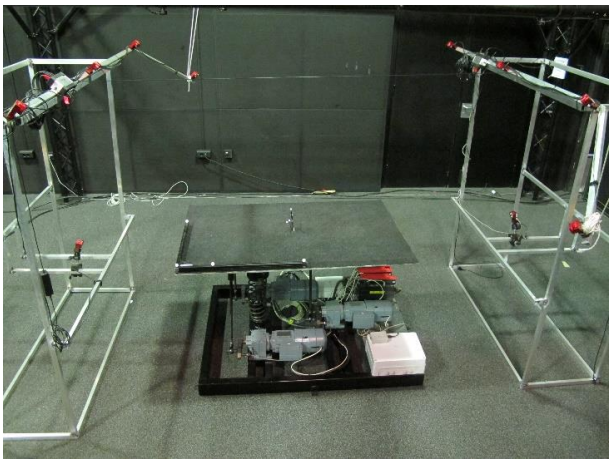

Fig. 3. The T1R2 heave-pitch-roll parallel manipulator implemented in our lab. The *Optitrack* tracking system can be seen at both sides of the motion platform. Its cameras track the position of the grey markers placed on top of the motion platform.

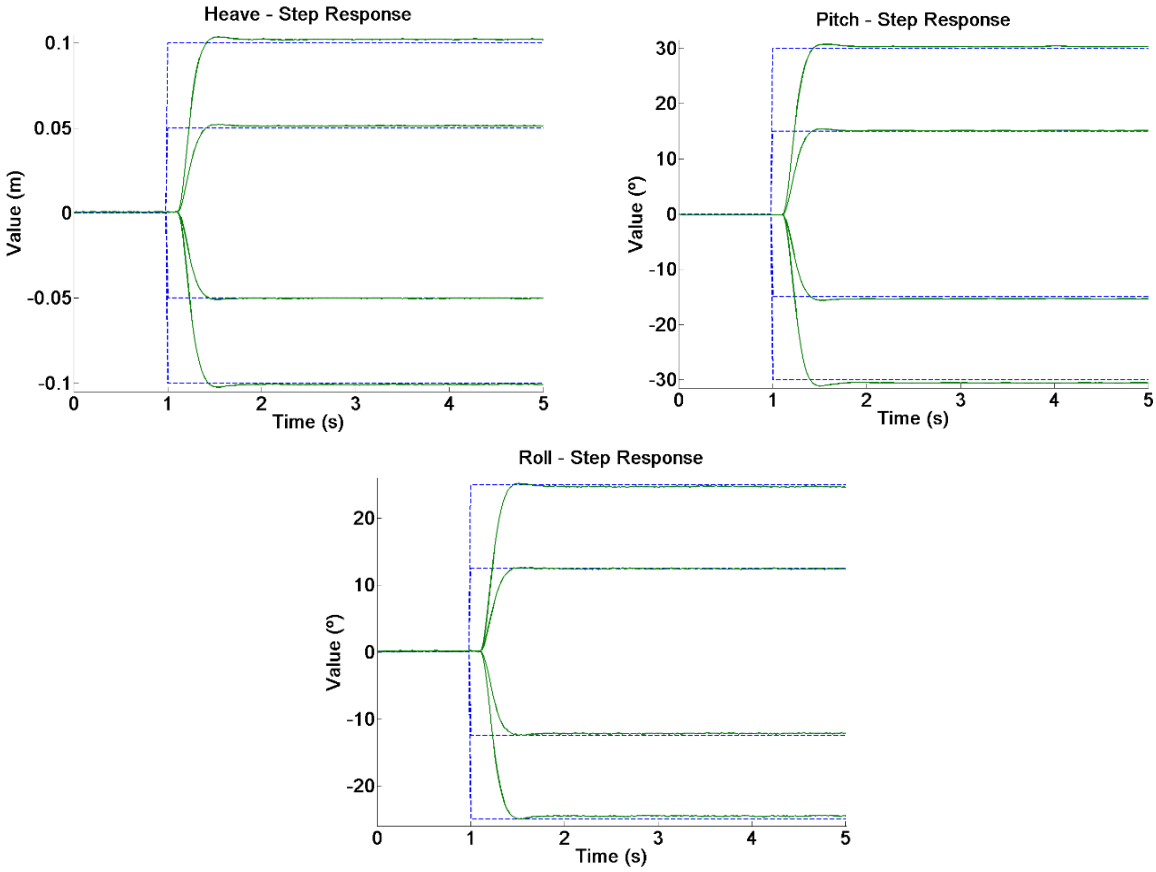

Fig. 4. Validation of the Inverse Kinematics for the three DOF, where: a) heave; b) pitch; and c) roll. Blue lines represent the commanded/theoretical (input) position/angles. Green lines represent the actual response (output) of the motion device.

5. Analysis of the reachable workspace and DOF interdependencies

5.1. Preliminary analysis

Once the IK formulation has been validated, it is advisable to analyze the available workspace of the T1R2 motion platform, because the smaller the reachable workspace, the harder is to generate believable motion cues. This section describes the process needed to perform this necessary step. The main idea is to analyze, not only the available reachable

[DOI: 10.1299/jamdsm.2017jamdsm0023]

DOF workspace, but also to study the relationship between the different DOF. As we are analyzing a 3-DOF motion platform, the whole workspace can be drawn either in a 3D heave-pitch-roll plot, or in three two-dimensional (2-DOF) plots showing the interrelationship between the different DOF involved (heave-pitch, heave-roll and pitch-roll) by setting the remaining DOF to zero. Two-dimensional plots are visually easier to understand.

The same parallel manipulator design used for the validation process presented in section 4 has been chosen to perform this analysis. The workspace analysis consists of three stages:

Stage 1: Full search. The first stage is a full discretized guided exploration of the whole workspace with these limits and increments: Heave range = [-0.12 m, 0.12 m], with increments of 0.0001 m; Pitch range = [-35°, 35°], with increments of 0.1°; Roll range = [-35°, 35°], with increments of 0.1°. The ranges have been chosen manually by a previous inspection of possible maximum values. In this stage, each point within that space is tested against the IK (using the formulation described in section 3) to know whether it could be reached by the manipulator (*feasible* = yes) or not. Then, the border line between reachable and unreachable poses is drawn.

Stage 2: Two-dimensional plots. The second stage is the same full guided exploration of the workspace with the same limits but in a 2-DOF space. First, the roll is set to 0° and then the heave-pitch space is traversed. Then, the same is repeated for the heave-roll space by setting pitch to 0°, and finally for the pitch-roll space by setting heave to 0 m.

Stage 3: Safe-zone search. As the workspace of a PM is usually a non-orthogonal shape, it is difficult for MCA to be tuned for the particular workspace of a motion platform (Reid and Nahon, 1986). This can cause that the device reach its limits repeatedly, as a good tuning of the MCA is hard to achieve when its limits are unknown or hard to enforce. When that happens, the MCA has to find a downscaled set of DOF if the desired ones are not reachable. If so, false inertial cues are generated, reducing the physical validity of the simulator (Reymond and Kemeny, 2000).

Even if the shape of the workspace is known, MCA are usually arranged in channels (Reid and Nahon, 1985) where each channel represents one translational or rotational DOF. Moreover, the tuning of each channel is usually performed individually (Grant, 1996), as it is rather complicated to deal with all of them at the same time. The problem then is that, with parallel manipulators, some DOF may be reachable for some input signals, but not all at the same time. For instance, we could reach 25° of pitch (with no roll) and we could also get 25° of roll (with no pitch), but we may not be able to obtain both 25° of pitch and 25° of roll simultaneously. This feature is an inherent consequence of most parallel designs.

This leads us to identify one of the main problems of motion cueing generation in motion simulation: MCA channels are usually set up separately but PM DOF are deeply interdependent. This fact makes MCA harder to set up with these manipulators, for unreachable combinations of DOF have to be downscaled and actuators limited. The limitation or downscale process can be complex (Schwarz, 2007) if the loss of inertial cues needs to be minimized. It is, thus, very interesting to define a safe zone in which the MCA could operate without having to worry about DOF interdependence, avoiding the need to downscale any DOF. This workspace subset would greatly simplify the MCA tuning and use. However, the problem of this safe-zone may be an under-use of the device, as many reachable DOF may not be used. Therefore, it is important to optimize this safe zone by making it as large as possible.

In the case of the manipulator being analyzed, the easiest way to define this safe zone is to specify six values: maximum heave, minimum heave, maximum pitch, minimum pitch, maximum roll and minimum roll, inside of which, any combination of DOF can be reached simultaneously. This defines an axis-oriented hyper-rectangle that may or may not be centered at the (0, 0, 0) of the workspace. In addition, for motion simulation, it is usually required that this safe zone contain the same positive and negative limits. Thus, this hyper-rectangle should be symmetric in an axis-by-axis basis. For instance: (-0.05 m, +0.05 m) for heave, (-20.0°, +20.0°) for pitch, and (-15.0°, 15.0°) for roll. This is usually the case, because MCA usually works with frequency filters that are symmetric. If symmetry is not necessary, only the largest possible axis-oriented hyper-rectangle is needed, and we can get, for instance, something like: (-0.05 m, +0.08 m) for heave, (-12.0°, +16.0°) for pitch, and (-15.0°, 11.0°) for roll.

Therefore, the third stage of the analysis is a Monte Carlo approach in order to search for the largest symmetric axis-oriented hyper-rectangle within the workspace, and also a similar search for the largest asymmetric axis-oriented hyper-rectangle. The resulting plots of this three-stage process can be seen in Fig. 5.

The analysis of the workspace, using the original equations, reveals some useful information. First, the workspace (blue points and lines) turns out to be a rotated box. As it was expected, the workspace is not orthogonal to the different DOF axes. Moreover, this box is not even centered at the (0, 0, 0), as it can be seen in the different 2-DOF (heave-pitch, have-roll, pitch-roll) plots. Figure 5 depicts non-symmetrical relationships among the different DOF (specially the pitch-roll one). The (0, 0, 0) mark is plotted with a red circle, and the actual center of the manipulator workspace, with a blue

[DOI: 10.1299/jamdsm.2017jamdsm0023]

circle. The larger the difference between the two, the least symmetric the workspace is.

Second, the heave range is not symmetric, and its shape is such that it is hard to cover with an axis-oriented rectangle. The largest possible axis-oriented symmetric rectangles are plotted with a pink dashed line, while the largest asymmetric ones are plotted in green dashed lines. The largest three-dimensional asymmetric hyper-rectangle (safe zone) is also plotted with a blue-red box inside the blue box-shaped workspace.

And third, maximum pitch cannot be reached with zero heave, which is not positive for the MCA, because the downscale of the DOF will be harder to implement. The same occurs with heave-roll and with pitch-roll.

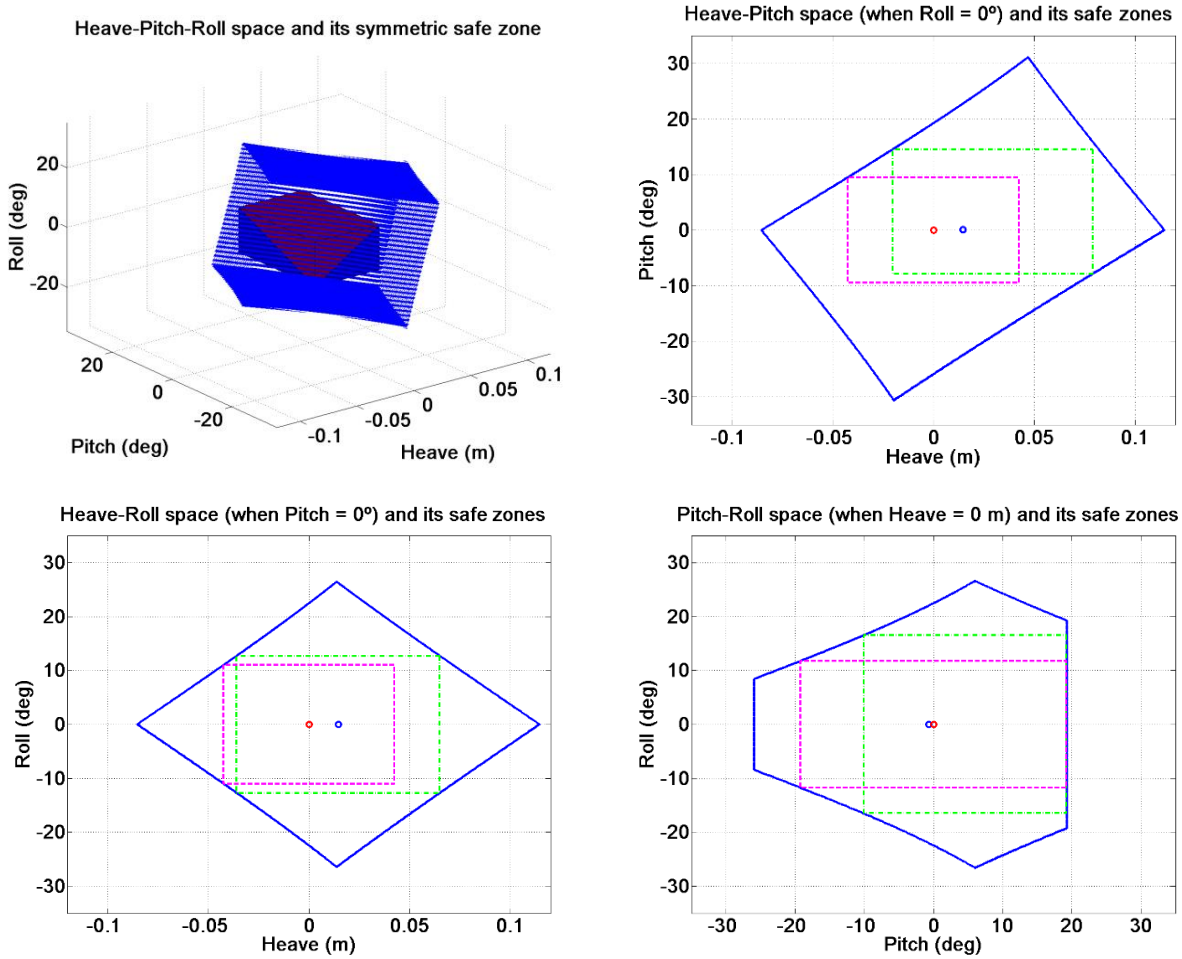

Fig. 5. Reachable workspace of the T1R2 mechanism. The top-left plot shows the three-dimensional workspace. The rest show two-dimensional plots setting the missing DOF to zero. Blue lines represent the boundaries of the reachable workspace. Pink rectangles show the maximum axis-oriented symmetric rectangles (safe zones) that can be found. Green rectangles show the largest asymmetric rectangles. A red dot marks the (0, 0, 0). A blue dot indicates the center of the workspace.

5.2. Improvements on the original reachable workspace for motion cueing generation

5.2.1. Analysis of heave offset

In order to understand why the heave range is not symmetric, it is first necessary to observe the heave limits. Figure 6 shows the heave range and its corresponding maximum and minimum values. The maximum and minimum distances between the upper and the lower triangle are $(p + r)$ and $(p - r)$ respectively. Therefore, the heave range is $2r$.

To properly check if the heave range is symmetric, it is useful to analyze first the home position. If the home position (heave = 0) is defined when $\alpha_1 = \alpha_2 = \alpha_3 = 0°$, then the distance between the two triangles, at this home position, can be calculated using Eq. (1). Therefore (see Fig. 6), heave limits and range can be calculated as:

[DOI: 10.1299/jamdsm.2017jamdsm0023]

$$\text{heave}_{\max} = (p + r) - h_0 = r + (p - h_0) = r + (p - \sqrt{p^2 - r^2}) \tag{14}$$

$$\text{heave}_{\min} = -(h_0 + r - p) = -r + (p - h_0) = -r + (p - \sqrt{p^2 - r^2}) \tag{15}$$

$$\text{heave}_{\text{range}} = \text{heave}_{\max} - \text{heave}_{\min} = r + (p - h_0) - \left(-r + (p - h_0)\right) = 2r \tag{16}$$

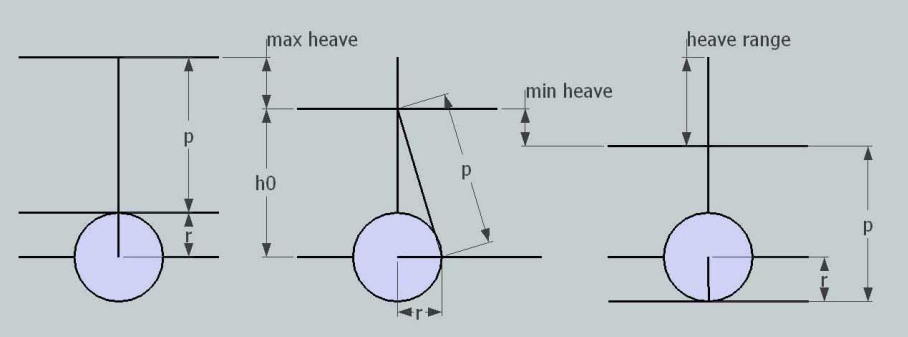

Fig. 6. Heave range. The left drawing represents the maximum heave (highest possible position of the moving base). The right drawing represents the minimum heave (lowest possible position). The drawing depicted in the middle represents the situation where the motors are in horizontal position.

Thus, the range is not symmetric $(-r,\ r)$ because of the term $(p - h_0)$, which causes an offset. This happens if the home position is defined when $\alpha_1 = \alpha_2 = \alpha_3 = 0°$. Then, with zero heave, the distance between the two triangles is h_0, instead of p, which would be the middle point of the range. As $h_0 \neq p$, this point does not represent the middle point of the range. The limit case (most asymmetric situation) occurs when $p = r$. In this case, $h_0 = 0$, lower and upper triangle coincide at home position, maximum heave is $p + r = 2r$, and minimum heave is $p - r = 0$. In a general case, this heave offset causes a difference between the real middle point (h_0) and the desired middle point (p) of the heave range. This difference can be easily calculated:

$$\text{heave}_{\text{offset}} = p - h_0 = p - \sqrt{p^2 - r^2} \tag{17}$$

Thus, the condition to get a symmetric heave range is to achieve a zero offset. This is accomplished when:

$$p^2 = p^2 - r^2 \tag{18}$$

This condition is only met when $r = 0$ or $p = \infty$. If $r = 0$, there will be no motion at all, and making p too long is not practical, so another solution is needed. A possible solution is to redefine the zero heave mark by subtracting the offset $(p - h_0)$ prior to the calculation of the IK. This causes the zero heave to occur at some angle $\alpha_1 = \alpha_2 = \alpha_3 = k \geq 0°$ (k will be calculated by IK and it does not really matter to us), and thus, the home position ($\alpha_1 = \alpha_2 = \alpha_3 = 0°$) will no longer cause the (0, 0, 0) position of the workspace. It is important to understand that, for this solution to work, there is no need to change the previous IK equations; we just need to calculate and subtract the heave offset $(p - h_0)$ before applying it to the IK equations. This way, there will be a symmetric $(-r, r)$ heave range. If this change is applied and the workspace analysis is repeated, the results are quite different. They are depicted in Fig. 7.

Heave range is now symmetric, as expected, and the heave-roll relationship is also much more symmetric. However, the heave-pitch relationship is still quite odd. For instance, to get the maximum pitch (about 30°), heave should be around 0.04 m, which seems quite counterintuitive.

[DOI: 10.1299/jamdsm.2017jamdsm0023]

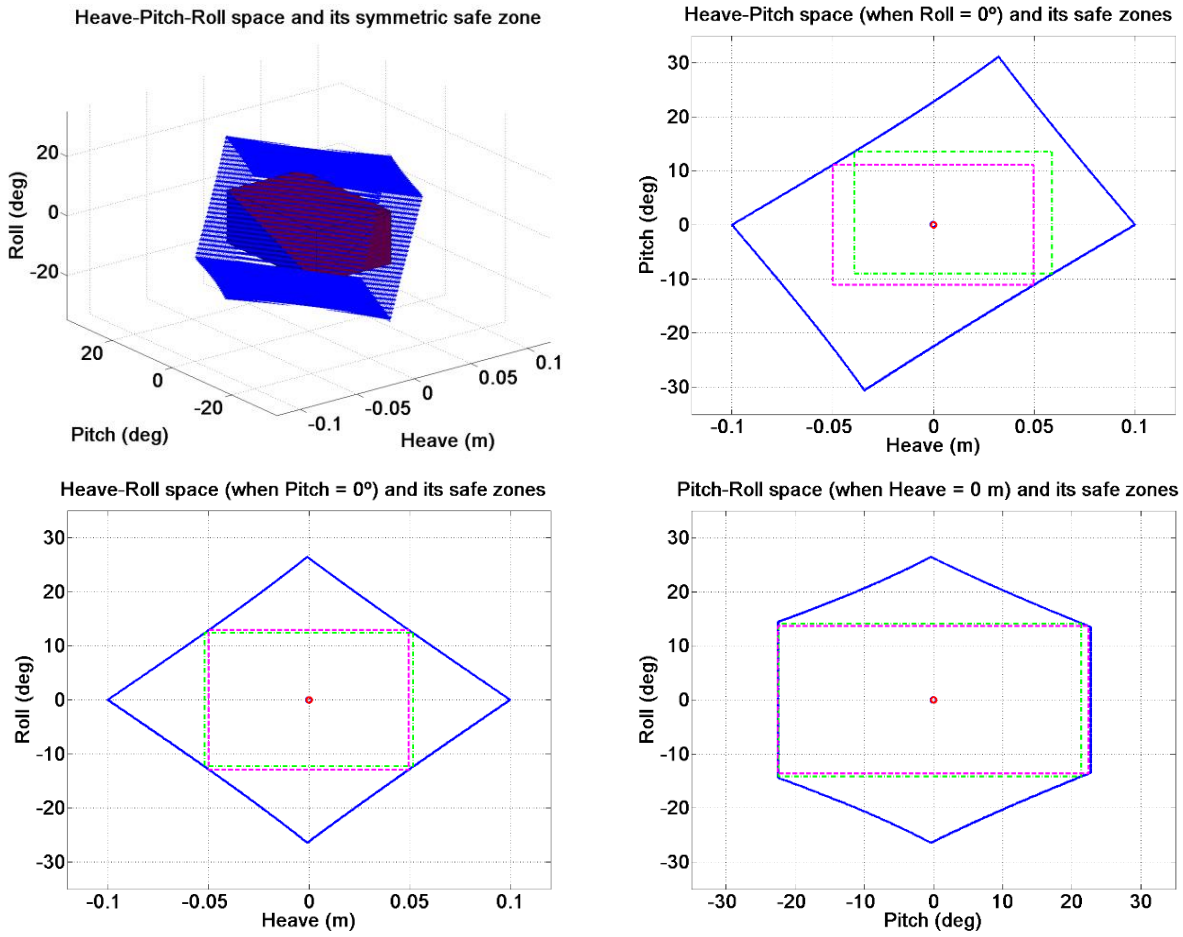

Fig. 7. Reachable workspace after the elimination of the heave offset. Information is depicted as in Fig. 5.

5.2.2. Analysis of the heave-pitch relationship

The anomaly shown in the heave-pitch relationship depicted in Fig. 5 and Fig. 7 comes from the upper triangle. Dynamically, an equilateral triangle provides full symmetry and load balance on the motors. Thus, it seems the right choice. Regarding the triangle center, in an equilateral triangle, the orthocenter, barycenter, circumcenter and incenter coincide at the same point. Thus, this point seems the natural choice to place the coordinate system. However, the barycenter is not the best place to locate this system. The reason is that, if this decision is taken, we will be assuming that the upper triangle rotates around this point, which is simply not true. This may seem a little counterintuitive (as the vertical splined shaft passes through the barycenter), but as the joint between the moving base and the vertical shaft is a prismatic universal joint, the moving base is not constrained to rotate around the universal joint anchor, because the vertical freedom allows the moving base to move up and down and, thus, rotate around a different point. This means that, if the barycenter is set as the center of the upper triangle, pitch cannot reach its peak value with heave set to zero, because to obtain the maximum pitch a little heave is necessary, due to the offset between the real center of rotation and the origin of the coordinate system. This rotation offset does not invalidate the equations; it just changes the relationship between the DOF, making them a little more complicated to understand and use, because a simple pitch rotation is 'seen' by the proposed coordinate system as a heave displacement plus an angular displacement (pitch).

If we assume that a piston is several times longer than a rod, which is usually the case, then, it can be assured that the base will rotate with respect to a point half distance from the triangle height (in the Y-axis) and half distance from the triangle base (in the X-axis). Thus, if that middle point is used as the center of the triangle (in the equations, not in the building process), pitch rotations will not imply heave displacements, pitch-heave plots will be symmetric, and more importantly, pitch will be able to get its maximum possible value when heave and roll are zero, because the rotation offset will be very close to zero (see Fig. 8). If the piston and rod are of similar sizes, a little offset error is present, but if the piston is long enough, this point will make the pitch-heave and pitch-roll relationship almost completely symmetric.

[DOI: 10.1299/jamdsm.2017jamdsm0023]

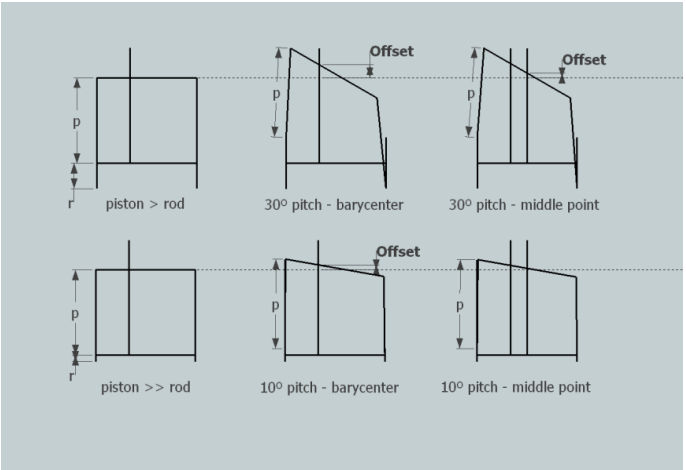

Fig. 8. Pitch rotation offset as seen from an YZ plane. Top drawings shows the case where the length of the piston is not many times longer than the length of the rod. The difference between using the barycenter (large offset) and the middle point (small offset) is shown. The three drawings in the bottom represent the situation where the length of the pistons is many times longer than the length of the rod. The offset is very much reduced (almost zero) when using the middle point.

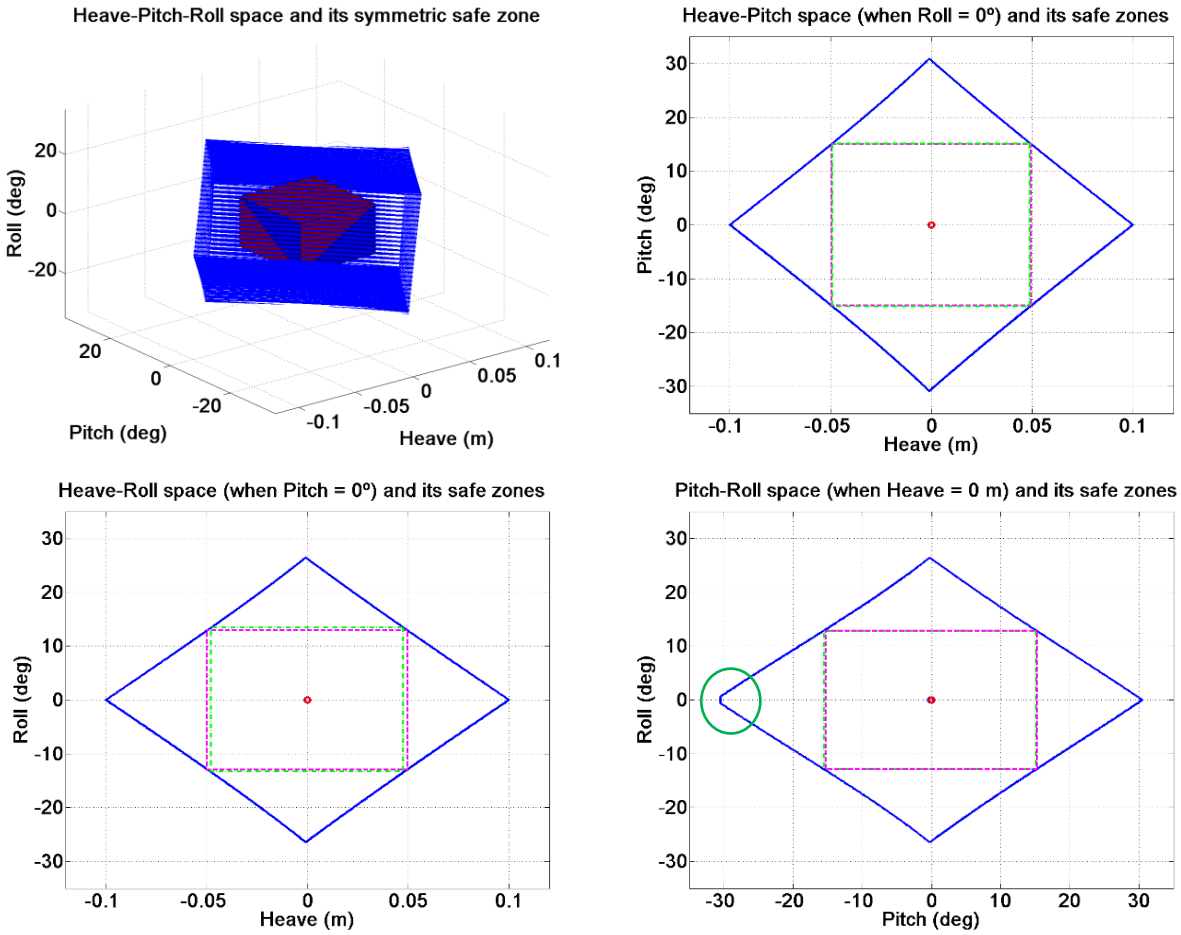

Fig. 9. Reachable workspace using a new triangle center. Heave offset is also previously eliminated. Information is depicted as in Fig. 5. Only a very small asymmetry is found in the left part of the pitch-roll plot (marked with a green circle).

Although the barycenter will still be used for building the motion platform and place there the vertical splined shaft and (possibly) a spring, this new middle point will be used as the center of the coordinate system. Again, this change does not imply to rewrite the IK equations. It just changes the value of some of its parameters (in particular $\overrightarrow{L_k}$ and $\overrightarrow{U_{k0}}$) because of the change of the location of the origin of the coordinate system. With this new coordinate system, the DOF

[DOI: 10.1299/jamdsm.2017jamdsm0023]

analysis can be repeated and, now, the workspace presents a much more appealing shape (see Fig. 9). Now, every single DOF is able to get its maximum value when the other two are set to zero. Whether this change makes the safe zone larger is something that needs to be analyzed yet, but the fact that every DOF can get its maximum value when the others are zero, is something that eases the design of an MCA. It is important to emphasize again that by applying the aforementioned changes, neither the manipulator, nor the equations, nor the DOF ranges have changed. They have only been rearranged in order to obtain an easier-to-use workspace by modifying the DOF-to-DOF relationship.

Finally, in order to analyze the effect of making the piston very long, the same analysis was performed but with a 10 m long piston (see Fig. 10). The figures are pretty much alike. The only difference is that the small asymmetry in the pitch-roll plot (left side of the pitch-roll plot in Fig. 9) relationship is not present. Thus, the conclusion is that the piston length does not modify the motion platform capabilities. It just rearranges the relationship between the different DOF.

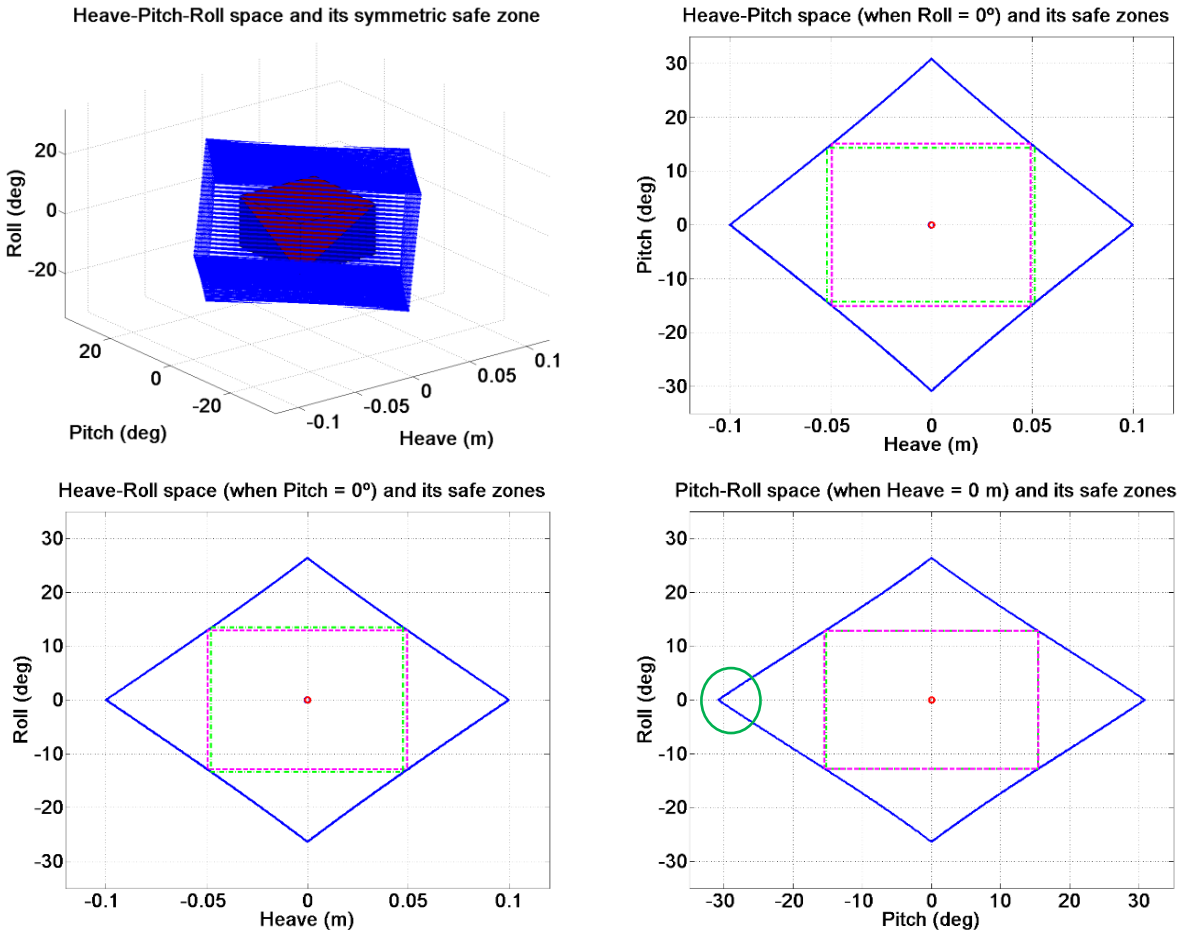

Fig. 10. Reachable workspace with a very long piston (10 m). Heave offset is also previously eliminated; the middle point is used as the triangle center. Information is depicted as in Fig. 5. The changes with respect to Fig. 9 are almost inappreciable. The only change is highlighted by a green circle. Making the piston many times longer than the rod completely eliminates the small pitch-roll asymmetry.

5.2.3. The piston/rod length ratio

As previously seen, the piston-rod length ratio, p/r, influences the relationship between the DOF and modifies the amount of heave offset that should be corrected. In order to understand the importance of the p/r ratio, we prepared an experiment where the effect of this quantity is shown. Table 1 shows the maximum and minimum possible values of one DOF when the other two are set to zero, setting r = 0.1, while varying p. The figures are obtained without performing the heave offset correction explained in section 5.2.1, but using the middle point (not the barycenter) as the center of the coordinate system. As it can be seen, as the p/r ratio gets closer to unity, the relationship between the DOF gets significantly less convenient for motion cueing.

[DOI: 10.1299/jamdsm.2017jamdsm0023]

Table 1. Effect of the p/r ratio (heave offset not corrected) on DOF relationship (r = 0.1).

p/r	Heave [m]	Pitch [deg]	Roll [deg]
10000	[-0.10000, 0.10000]	±30.886	±26.389
100	[-0.99951, 0.10049]	±30.720	±26.259
10	[-0.09501, 0.10500]	±29.282	±25.042
5	[-0.08999, 0.11000]	±27.634	±23.679
2	[-0.07322, 0.12677]	±22.229	±19.197
1.1	[-0.03579, 0.16411]	±10.613	±9.280

This effect is much less important, although it is still present, if the heave offset is eliminated using the correction explained in section 5.2.1. Table 2 shows the values of a similar experiment, but correcting first the heave offset (the triangle is still centered on the middle point, not in the barycenter). The conclusion is that the effects of the p/r ratio are important, but could be mitigated if proper actions are taken. In any case, it is advisable that the piston be several times longer than the connecting rod.

Table 2. Effect of the p/r ratio (heave offset corrected) on DOF relationship (r = 0.1).

p/r	Heave [m]	Pitch [deg]	Roll [deg]
10000	[-0.10000, 0.10000]	±30.886	±26.389
100	[-0.10000, 0.10000]	±30.871	±26.375
10	[-0.10000, 0.10000]	±30.750	±26.316
5	[-0.10000, 0.10000]	±30.629	±26.257
2	[-0.10000, 0.10000]	±30.266	±26.140
1.1	[-0.10000, 0.10000]	±29.827	±26.038

5.2.4. Analysis of the safe zones

The final step of our study is the analysis of the volumes (or areas) of the safe zones (axis-oriented hyper-rectangles) for the different configurations. Obviously, the larger the safe zone is, the better for future MCA use. Table 3 shows the volumes of the symmetric safe zones (symmetric axis-oriented hyper-rectangles) for the different configurations analyzed in sections 5.1, 5.2.1, and 5.2.2. Configurations 1, 2, 3 and 4 correspond to the configurations shown in Figs. 5, 7, 9 and 10, respectively. HPR stands for heave-pitch-roll, HP means heave-pitch, HR is heave-roll and PR means pitch-roll.

Table 3. Largest symmetric hyper-rectangles volumes and areas.

	HPR [m* deg^2]	HP[m*deg]	HR [m*deg]	PR [deg^2]
Config. 1 (original)	21.58	1.6167	1.8705	906.70
Config. 2 (no heave offset)	34.69	2.2177	2.5663	1225.60
Config. 3 (new triangle center)	22.63	2.9702	2.5663	781.60
Config. 4 (very long piston)	22.72	2.9738	2.5680	791.40

As it can be seen, the original configuration (1) is the worst one in terms of HPR volume. Configuration 2 is the one with the largest symmetric hyper-rectangle. Configurations 3 and 4 are very similar, but better than configuration 1. Their HP and HR safe zones are the largest, but the HPR hyper-rectangle and the PR rectangle are smaller than those of configuration 2. Table 4 shows the same study, but with asymmetric safe zones (asymmetric axis-oriented hyper-rectangles), which are, in general, less preferable because an MCA does not usually expect any asymmetry.

As shown, configurations 1 and 2 are now the ones with the largest volumes for the whole HPR space. Configurations 3 and 4 remain far. Now, configuration 4 is not better than configuration 3. Obviously, as configuration 4 is the most symmetric, there is very little gain in using an asymmetric safe zone. Moreover, now, configuration 2 is similar to configuration 1 for every case except for the PR case, where configuration 2 is, by far, the best one. It can also be seen that some of the asymmetric hyper-rectangles are slightly smaller than the symmetric ones. This is a result of the Monte

[DOI: 10.1299/jamdsm.2017jamdsm0023]

Carlo method, which introduces a small error.

Table 4. Largest asymmetric hyper-rectangles volumes and areas.

	HPR [m* deg^2]	HP [m*deg]	HR [m*deg]	PR [deg^2]
Config. 1 (original)	34.16	2.2245	2.5548	964.64
Config. 2 (no heave offset)	33.12	2.2191	2.5482	1238.67
Config. 3 (new center)	22.15	2.9552	2.5489	785.25
Config. 4 (very long piston)	22.15	2.9518	2.5588	784.37

In conclusion, the decision to use configuration 2 or configuration 3 (configuration 4 is impractical) would be based on the importance of having a symmetric heave-pitch relationship. If this is needed, configuration 3 would be used. If not, configuration 2 would be chosen instead of configuration 1, as it maximizes the safe-zone, both using symmetric and asymmetric hyper-rectangles, and because it produces a symmetric heave range. The assessment of a certain safe volume allows motion platform designers to tune up MCA software without having to worry about DOF interdependence. MCA are already hard enough to tune, so it is very important to get rid of this interdependence problem, even at the cost of wasting some of the workspace. This allows MCA designers to tune each DOF independently and be sure that "what you ask is what you get", i.e. no DOF downscaling will ever occur if the tuning process is done properly at each DOF.

It is important to emphasize that this analysis is useful to achieve a better kinematic use of the PM. However, the dynamic performance of a motion platform depends on the physical properties of the actuators and on the MCA that make use of this mechanism. They also depend on the real motion data to feed the MCA, so that the PM can produce motion that is substantially similar to the expected one. In any case, this kinematic analysis is the first step for improving the capabilities of motion platforms and surely helps improving also the dynamic behavior. The topic of evaluating and tuning an MCA is a very complicated one, since the problem is subjective but objective measurements are required to perform fair comparisons between different devices. There is a broad literature on the topic that readers could consult (Hosman and Advani, 2016; Zaal et al., 2015). An example of this kind of analysis can be found in (Casas et al., 2015) where real vehicle data is used. However, a limit between good a bad motion cueing is hard to establish.

6. Conclusions and future work

In this paper, the reachable workspace of a 3-DOF T1R2 heave-pitch-roll parallel manipulator has been analyzed, always keeping in mind that our aim is to analyze only the kinematic capabilities of this parallel manipulator when used as a motion cueing generator in vehicle simulations. Other important considerations such us dynamic performance, dexterity, accuracy, singularity analyses, repeatability and reliability are kept aside, and left for further studies.

The selected manipulator is a common device in low-cost commercial motion cueing solutions. For this device, the shape of its workspace (and how the different parameters and design considerations affect it) has been analyzed. Moreover, a number of changes, in order to obtain a more suitable DOF-space for motion cueing generation, are also provided and justified after a detailed analysis. To perform this study, it is first necessary to solve the Inverse Kinematics of the manipulator. The results of this analysis showed that the original IK formulation presents some non-desirable features. First, the heave range is asymmetric. Second, the maximum values of pitch and roll cannot be reached when heave is set to zero. And finally, the workspace is not orthogonal to the DOF axes and it is not centered.

We studied how these results could be improved in order to ease the use of the manipulator by an MCA, drawing the following conclusions. Regarding the asymmetry of the heave range, it was proved that there is a small heave offset that could be eliminated by simply redefining the home position used in the IK calculations. Regarding the heave-pitch relationship, it was shown that the problem was the choice of the barycenter as the center of the upper triangle and the origin of the IK coordinate system. Instead of choosing the barycenter, a new center at half distance from the triangle height was proposed. The main result is that, the center of the DOF coordinate system affects the relationship between the DOF. It was also shown that piston length does not modify the motion platform capabilities but affects the relationship among the different DOF. Finally, regarding the workspace not being orthogonal to the DOF axes and not being centered, this is something unavoidable. Nevertheless, we analyzed the volume of the safe zones and showed two possible configurations that provide an easier use of the PM for motion cueing. The choice of the appropriate configuration will depend on the importance of either having a symmetric heave-pitch relationship or maximizing the use of the workspace.

[DOI: 10.1299/jamdsm.2017jamdsm0023]

Although particular conclusions are drawn for this PM, the performed analysis and most of the concepts proposed here can be used or extrapolated for other motion platforms. Moreover, the analysis includes objective measures on the workspace volume that can provide a simple but effective way of comparing different kinds of motion platforms for this particular use.

Future work includes analyzing a different manipulator, for instance a 2-DOF low cost manipulator, or some other 3-DOF MP with a different structure. A dynamic analysis of the response of the manipulator over time can also be performed. In addition, the influence of the construction parameters of the motion platform in the induced presence on human users can also be studied. Last, but certainly not least, a detailed singularity analysis of the manipulator would be interesting.

References

Arioui, H., Hima, S. and Nehaoua, L., 2 DOF Low Cost Platform for Driving Simulator: Modeling and Control, Proceedings of the 2009 IEEE/ASME International Conference on Advanced Intelligent Mechatronics (2009), pp.1206-1211.

Callegari, M., Palpacelli, M. and Principi, M., Dynamics modelling and control of the 3-RCC translational platform, Mechatronics, Vol.16, No.10 (2006), pp.589-605, doi: 10.1016/j.mechatronics.2006.06.001.

Callegari, M. and Tarantini, M., Kinematic Analysis of a Novel Translational Platform, Journal of Mechanical Design, Vol.125, No.2 (2003), pp.308-315, doi: 10.1115/1.1563637.

Casas, S., Coma, I., Portalés, C. and Fernández, M., Towards a simulation-based tuning of motion cueing algorithms, Simulation Modelling Practice and Theory, Vol.67 (2016), pp.137–154, doi: 10.1016/j.simpat.2016.06.002.

Casas, S., Coma, I., Riera, J. V. and Fernández, M., Motion-Cuing Algorithms: Characterization of Users' Perception, Human Factors: The Journal of the Human Factors and Ergonomics Society, Vol.57, No.1 (2015), pp.144-162, doi: 10.1177/0018720814538281.

Cheng, Y., Ren, G. and Dai, S., The multi-body system modelling of the Gough–Stewart platform for vibration control, Journal of Sound and Vibration, Vol.271, No.3 (2003), pp.599-614.

Dasgupta, B. and Mruthyunjaya, T. S., The Stewart platform manipulator: a review, Mechanism and Machine Theory, Vol.35, No.1 (2000), pp.15-40, doi: 10.1016/S0094-114X(99)00006-3.

Di Gegorio, R., Kinematics of the translational 3-URC mechanism, Proceedings of the 2001 IEEE/ASME International Conference on Advanced Intelligent Mechatronics Vol.1 (2001), pp.147-152.

Dingxuan, Z., Hironao, Y., Takayoshi, M. and Haidong, H. H. K., A new method of presenting realistic motions for a 3-degree-of-freedom motion base applied in virtual reality system, Paper presented at the Fifth International Conference on Fluid Power Transmission and Control ICFP (2001), Hangzhou, China.

Gogu, G., Fully-isotropic parallel manipulators with five degrees of freedom, Proceedings of the IEEE International Conference on Robotics and Automation ICRA (2006), pp.1141-1146.

Grant, P. R., The Development of a Tuning Paradigm for Flight Simulator Motion Drive Algorithms, Ph.D (1996), University of Toronto, Toronto, ON, Canada.

Groen, E. L. and Bles, W., How to use body tilt for the simulation of linear self motion, Journal of Vestibular Research, Vol.14, No.5 (2004), pp.375-385.

Hosman, R. and Advani, S., Design and evaluation of the objective motion cueing test and criterion, The Aeronautical Journal, Vol.120, No.1227 (2016), pp.873-891.

InMotion, InMotion Simulation - Moving the World (online), available from <http://www.inmotionsimulation.com>, (accessed on 8 April, 2017).

Kim, J. Y., Task based kinematic design of a two DOF manipulator with a parallelogram five-bar link mechanism, Mechatronics, Vol.16, No.6 (2006), pp.323-329, doi: 10.1016/j.mechatronics.2006.01.004.

Kong, X. and Gosselin, C. M., Kinematics and singularity analysis of a novel type of 3-CRR 3-DOF translational parallel manipulator, Int. Journal of Robotic Research, Vol.9, No.791 (2002).

Korobeynikov, A. V. and Turlapov, V. E., Modeling and Evaluating of the Stewart Platform, Paper presented at the International Conference Graphicon (2005), Novosibirsk: Akademgorodok.

Li, H., Gosselin, C. M. and Richard, M. J., Determination of the maximal singularity-free zones in the six-dimensional workspace of the general Gough–Stewart platform, Mechanism and Machine Theory, Vol.42 (2007), pp.497-

[DOI: 10.1299/jamdsm.2017jamdsm0023]

511.

Liu, K., Fitzgeralk, J. M. and Lewis, F. L., Kinematic Analysis of a Stewart Platform Manipulator, IEEE Transactions on Industrial Electronics, Vol.40, No.2 (1993), pp.282-293.

MacNeilage, P. R., Banks, M. S., Berger, D. R. and Bulthoff, H. H., A Bayesian model of the disambiguation of gravitoinertial force by visual cues, Experimental Brain Research, Vol.179, No.2 (2007), pp.263-290, doi: 10.1007/s00221-006-0792-0.

Majid, M. Z. A., Huang, Z. and Yao, Y. L., Workspace Analysis of a Six-Degrees of Freedom, Three-Prismatic-Prismatic-Spheric-Revolute Parallel Manipulator, Vol.16 (2000), pp.441-449, Springer London.

Merlet, J. P., Parallel Robots (2006), Springer, The Netherlands.

Nahon, M. A. and Reid, L. D., Simulator motion-drive algorithms - A designer's perspective, Journal of Guidance, Control and Dynamics, Vol.13, No.2 (1990), pp.356-362, doi: 10.2514/3.20557.

Nehaoua, L., Mohellebi, H., Amouri, A., Arioui, H., Espié, S. and Kheddar, A., Design and Control of a Small-Clearance Driving Simulator, IEEE Transactions on Vehicular Technology, Vol.57, No.2 (2008), pp.736-746.

Pouliot, N. A., Gosselin, C. M. and Nahon, M. A., Motion simulation capabilities of three-degree-of-freedom flight simulators, Journal of Aircraft, Vol.35, No.1 (1998), pp.9-17.

Reid, L. D. and Nahon, M. A., Flight Simulation Motion-Base Drive Algorithms: Part 1 - Developing and Testing the Equations, Vol.296 (1985), University of Toronto: UTIAS.

Reid, L. D. and Nahon, M. A., Flight Simulation Motion-Base Drive Algorithms: Part 2 - Selecting the System Parameters, Vol.307 (1986), University of Toronto: UTIAS.

Reymond, G. and Kemeny, A., Motion Cueing in the Renault Driving Simulator, Vehicle System Dynamics: International Journal of Vehicle Mechanics and Mobility, Vol.34 (2000), pp.249-259.

Richard, P., Gosselin, C. M. and Kong, X., Kinematic Analysis and Prototyping of a Partially Decoupled 4-DOF 3T1R Parallel Manipulator, Journal of Mechanical Design, Vol.129, No.6 (2007), pp.611-616, doi: 10.1115/1.2717611.

Schwarz, C. W., Two Mitigation Strategies for Motion System Limits in Driving and Flight Simulators, IEEE Transactions on Systems, Man, and Cybernetics, Part A: Systems and Humans, Vol.37, No.4 (2007), pp.562-568.

Servos & Simulation, Servos & Simulation, Inc. - High Technology Engineering (online), available from <http://www.servos.com>, (accessed on 8 April, 2017).

Sinacori, J. B., The Determination of Some Requirements for a Helicopter Flight Research Simulation Facility, Vol.7805 (1977), Moffet Field, CA, USA.

Stewart, D, A Platform with six degrees of freedom, Proceedings of the Institution of Mechanical Engineers (1965).

Tsai, L.-W., Robot analysis: the mechanics of serial and parallel manipulators (1999), John Wiley & Sons.

Tsai, L. and Joshi, S., Kinematics and Optimization of a Spatial 3-UPU Parallel Manipulator, Journal of Mechanical Design, Vol.122, No.4 (2000), pp.439-446, doi: 10.1115/1.1311612.

Zaal, P. M. T., Schroeder, J. A. and Chung, W. W. Y., Objective Motion Cueing Criteria Investigation Based on Three Flight Tasks, Paper presented at the Challenges in Flight Simulation (2015), London, UK.

Zhang, Y., Liu, H. and Wu, X., Kinematics analysis of a novel parallel manipulator, Mechanism and Machine Theory, Vol.44, No.9 (2009), pp.1648-1657, doi: 10.1016/j.mechmachtheory.2009.01.006.

[DOI: 10.1299/jamdsm.2017jamdsm0023]